INVESTIGATIONS OF THE HYDRODYNAMIC FLOW FIELD IN THE DRAFT TUBE CONE OF THE HYDRAULIC TURBINES AND THE FLOW CONTROL WITH A MAGNETO-RHEOLOGICAL DEVICE

PhD. Thesis – Summary

for obtaining the scientific title of doctor at
Politehnica University of Timisoara
in the doctoral field of MECHANICAL ENGINEERING

candidate **author Eng. *Raul-Alexandru SZAKAL***
Scientific advisor Dr. Eng. Sebastian MUNTEAN, Senior Researcher

October 2023

Introduction

The main topic of this PhD thesis is the hydrodynamic instabilities inside the draft tube cone of hydraulic turbines and flow control using magneto-rheological devices. The thesis is structured in 8 chapters and the foundation of the analyzed topic consists of 203 references. The issues come from operating the hydraulic turbines outside of best efficiency point (BEP).

The hydropower still represents the biggest source of renewables [1]. This is due to their technical maturity and high efficiency. However, in the last 20 years, the renewable sources diversified, and photovoltaic and wind turbines are nowadays widely used. The contribution from sources as wind and solar in renewable production raised with about 23% between 2005-2018 [1]. Due to the non-permanent and fluctuant production of energy produced from this renewable source, major problems arise in terms of electrical grid stability. For this reason, hydraulic turbines are more often used for ancillary services (e.g., primary frequency control because of rapidity and high level of power regulation). However, when they are operated for power regulation of the grid, the hydraulic turbines operates very often at part load regimes and experience many start-stop cycles [2]. This defective operation leads to high dynamic loads on mechanical components of the hydraulic turbine. Moreover, the hydrodynamic instabilities that appear into the draft tube cone of the hydraulic turbines have negative impact on efficiency, leads to vibrations [3] and may cause failure of the mechanical components of the hydraulic turbine [4].

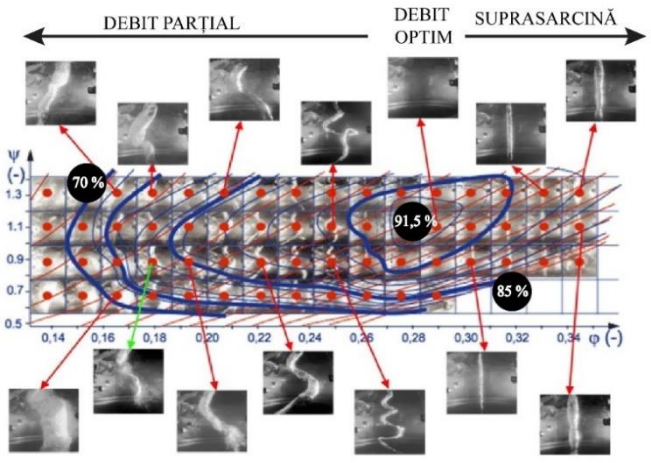

Figure 1. Instabilities from the draft tube cone of the Francis hydraulic turbine operated at different part load and full load regimes [5]

The macroscopic structures identified by Jacob [5] at off design operations of the Francis hydraulic turbines are presented in Figure 1. The most aggressive phenomena from unsteadiness point of view are those at part load regimes (70% from BEP) [6-9]. The macroscopic form of these phenomena is known as vortex rope or rotating vortex rope. Due to the processing motion of this instability, strong pressure pulsations were observed at the wall of the draft tube cone. The vortex rope usually wraps around a quasi-stagnant region [10-12].

To diminish or eventually eliminate the unfavorable effects of such phenomena, some control methods and techniques were proposed. A successfully flow control method should ensure 3 essential aspects: (i) to address the cause of the instabilities rather than effects, (ii) to not affect the efficiency of the hydraulic turbine when it is not operated and (iii) can be stopped when is not necessary to be used, in agreement with Kougias et. al. [2] . Two major classes of control technics are distinguished: passive control technics which do not require supplementary energy source and active control techniques that do require additional energy. The major disadvantage of using a passive technique is that in general requires major structural modification while for the active ones is the price of the supplementary energy required. Many of these flow control techniques are discussed in the PhD. thesis [13-20].

The vortex rope hydrodynamics and flow control technique with magneto-rheological device are studied in the thesis using a surrogate of Francis FLINDT hydraulic turbine called swirling flow generator [21], Figure 2. The swirling flow generator apparatus consists of two rows of blades, one fixed called guide vane and one in rotational motion called rotor. The two rows of blades are mounted together in a cylindrical test section and fixed on the hub by a nozzle. At the outlet of the rotor, a convergent divergent test section is mounted. The semi-angle of the cone of the divergent part is 8°. The rotor spins freely at 1020 rpm when a discharge of 30 l/s is vehiculated. The rotor was designed to induce an excess of kinetic energy near to the tip and a deficit near to the hub. In this way, the flow pattern from the Francis FLINDT hydraulic turbine operated at 70% from BEP is generated into the divergent section. Several operating regimes similar to the part load regimes from Francis turbine are obtained and analyzed by modifying the rotor speed of the swirl generator using a magneto-rheological device.

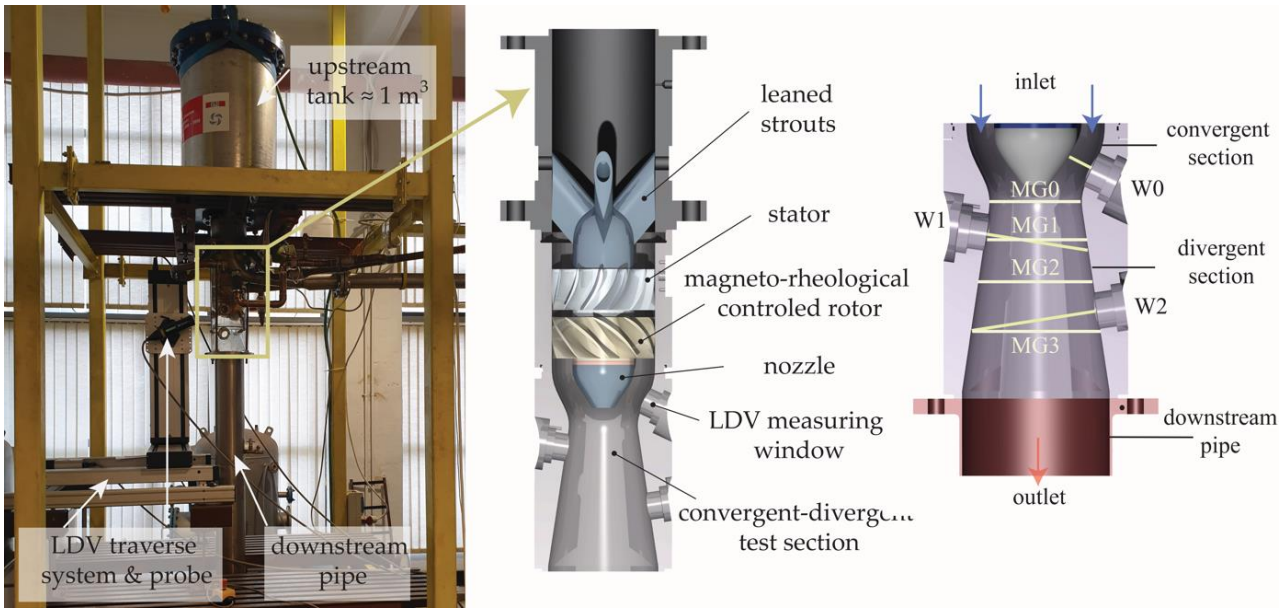

Figure 2 The experimental test rig and swirling flow generator together with the test section available at Faculty of Mechanics of University Politehnica Timisoara

The PhD. thesis aims to contribute to a better understanding of the hydrodynamic instabilities from the draft tube cone of the Francis hydraulic turbines at part load regimes. Both experimental

and numerical investigations were performed. The test rig for swirling flow investigations from Faculty of Mechanics of Politehnica University Timisoara was used for the experimental investigation. The test rig allows to quantify the flow features as unsteady pressure at the wall of the divergent test section and the mean velocity profiles downstream to the rotor through a 2D LDV measuring system. To a deeper understanding of the unsteady phenomena from the cone of the hydraulic turbines, computational fluid dynamics (CFD) was performed using the commercial Fluent 6.3 software.

The magneto-rheological flow control technique in hydraulic turbines is an innovative concept to extend their operating domains. To reach the aim of the thesis two specific objectives were defined:

i. Designing and testing a magneto-rheological flow control to modify the rotor`s speed of the swirling flow generator working underwater.

ii. Experimental and numerical investigation of 3D decelerated swirling flow downstream to the rotor of the hydraulic turbines to identify the source of the self-induced plunging type component in swirling flow.

Considering the previous objective, the thesis was structured in 8 chapters as follows:

Chapter 1. Introduction – involves a bibliography study to reach the state of the art in the operation of Francis hydraulic turbines at part load regimes, associated phenomena, flow control and in term of magnetorheological fluids and designing applications with it.

***Chapter 2. Magneto-rheological fluids device design to control the rotor`s speed of the swirling flow generator*** – describes the design methodology for the above-mentioned device and magneto-rheological behavior analysis of the selected magneto-rheological fluids (MRF`s). Two commercial MRF`s (MRF 132 DG and MRF 336 AG) produced by Lord Co. and a nano-micro composite in two concentrations (SMR 35% Fe + UTR Ms 1000 and 950 G produced by the Magnetic Fluids Laboratory of the Romanian Academy – Timisoara Branch) behavior were investigated using the Physica MCR300 rheometer available at Politehnica University Timisoara.

Chapter 3. Design methodology validation and investigation of the magneto-rheological brake device operated in air and water working environment – presents the design methodology validation with experimental data and the experimental results obtained using a 1:1 scale magneto-rheological brake device with the one used to control the rotor speed of the swirling flow generator.

Chapter 4. Experimental investigations of swirling flow in straight configuration at different part load regimes obtained using magneto-rheological control – presents the experimental investigations performed on the test rig for decelerated swirling flow from Faculty of Mechanics of Politehnica University Timisoara. The mean velocity components of the hydrodynamic field and the unsteady pressure pulsations are analyzed using the 2D Laser Doppler Velocimetry (LDV) and unsteady pressure sensors, respectively. Many operating regimes are obtained using the magneto-rheological brake device as flow control element.

Chapter 5. 3D numerical investigations of the self-induced hydrodynamic instabilities in straight configuration – presents the computational domain and setup for analyzing the operating regimes obtained in straight configuration in previous chapter and the validations of the CFD using experimental data. The aim of this analysis is to extend the understanding of the hydrodynamic instabilities from the draft tube cone of the hydraulic turbines operated at part load regimes.

Chapter 6. Analysis of the vortex rope morphology – using the results from the validated CFD experiment, in this chapter the unsteady evolution of the vortex core is analyzed for few operating points. The mechanisms that generate the low frequency plunging component are explained for monophase flow downstream the rotor of the swirling flow generator into the draft tube cone.

Chapter 7. Analysis of the hydrodynamic flow field and influence of draft tube elbow geometry on induced plunging component – presents the experimental investigations performed at

several operating points of the swirling flow generator while 3 simplified geometries of the draft tube heel elbow are mounted downstream.

Chapter 8. Conclusions, personal contributions and perspectives – presents an outline of the thesis together with the main conclusions regarding the conducted research, the main contributions and some possible future research directions regarding the studied topics.

The first step, realized in **chapter 2** to reach the objectives of the thesis was developing the magneto-rheological control device design methodology to control the rotor`s speed of the swirling flow generator.

The basic working principle of the magneto-rheological device consists of mounting a variable viscosity magneto-rheological fluid (MRF) into the gap placed between a fixed and a rotating part. Using an electromagnet placed close to the gap, a magnetic field is distributed perpendicular to the gap and the viscosity of the MRF increases. This effect is known as magneto-viscous effect and it is fast and reversible [22]. The steps followed in this chapter are:

i. bibliography study together with critical analysis about the advantages of using MRFs in control applications.
ii. defining the requirements for the targeted control application.
iii. identifying the design considerations such as geometry type selection, designing of the magnetic circuit, defining a relation between the MRF`s properties and the operating conditions of the design device.
iv. Magneto-rheological characterizations of the MRFs to better understand their behavior in the presence of magnetic field and to identify the characteristic parameters for design methodology developed.

Starting from the geometrical constraints available into the hub of the rotor of the swirling flow generator results for the design device that the ratio between the Rext/L = 0.67. The Rext and L are the exterior radius for the available volume and height, respectively. For this ratio, a double gap cylindrical configuration with one coil has been selected based on literature recommendations [23].

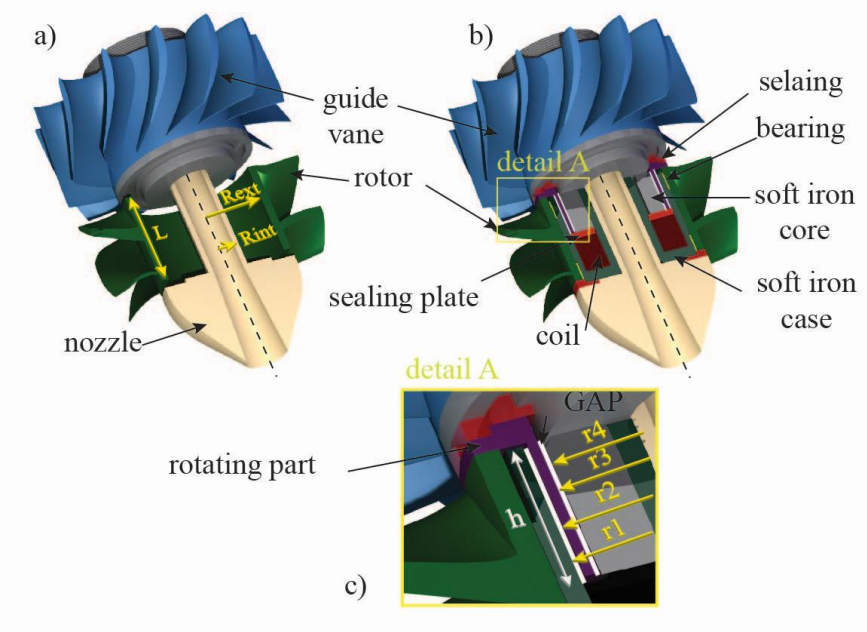

Figure 3. Section views of the rotor (a) the selected geometry for the magneto-rheological control device (b) detail view of the resulted gaps (c)

The magneto-rheological control device addresses controlling the flow regimes at quasi-stationary operating point. At these regimes, the hydrodynamic instability (e.g., vortex rope) is well

developed and the swirling flow generator is not operated in transitory regimes. For this reason, the dynamic response, and the activation time of MRFs is not of interest.

For controlling the rotor`s speed of the swirling flow generator up to 300 rpm, a total braking torque of 5.57 Nm at around 341 W is necessary based on numerical simulations [24]. The main requirement considered in the design stage is the braking torque of 5.57 Nm to be ensured just by the magneto-rheological braking contribution. Starting from viscosimeter concepts [25, 26], a relation for determining the magneto-rheological braking contribution was developed for the selected device geometry:

$$\mathbf{M} = 2\pi h r_2^2 \left(\frac{2\Omega}{\mathbf{p}}\right)^p c\left[1-\left(\frac{r_2}{r_1}\right)^{2/p}\right]^{-p} + 2\pi h r_3^2 \left(\frac{2\Omega}{\mathbf{p}}\right)^p c\left[1-\left(\frac{r_3}{r_4}\right)^{2/p}\right]^{-p} \quad (1)$$

where M is the braking torque generated by the shearing of the MRFs into the gaps (marked with white on Figure 3b), *c* and *p* are the characteristic parameters of the MRFs obtained with Power Law ($\tau = c\,\dot{\gamma}^P$) on flow curves, *r1...r4* are the radius from which the gap's dimensions result, *h* is the heigh of the gap and Ω is the angular velocity. This hypothesis considers that into the gaps a non-Newtonian fluid, in steady flow state, is sheared.

For studying the contribution of the developed relation, a simplified formula identified in literature has been used:

$$M = 2\pi h \tau(\dot{\gamma})(r_3^2 + r_2^2) \quad (2)$$

where $\tau(\dot{\gamma})$ it is the shear stress collected straight from the flow curves, and r_3,r_2 are the radius of the cylinder which rotates, see Figure 3c. This hypothesis considers that the MRF behavior is Newtonian.

4 MRFs have been selected initially for studying their magneto-rheological behavior. Two commercial MRF`s (MRF 132 DG and MRF 336 AG produced by Lord Corporation) and one nano-micro composite in two concentrations especially tunned for this application (SMR 35% Fe + UTR Ms 1000 G and SMR 35% Fe + UTR Ms 950 G produced by Magnetic Fluids Laboratory of the Romanian Academy – Timisoara Branch) were considered. Physica MCR 300 rheometer available at Faculty of Mechanics of Politehnica University Timisoara with plate-plate magneto-rheological cell has been used to characterize the 4 selected MRFs. Casson`s model ($\sqrt{\tau} = \sqrt{\tau_C} + \sqrt{\eta_C \dot{\gamma}}$) was used to quantify the dynamic yield stress $\tau_C$ and the Casson`s viscosity η_C.

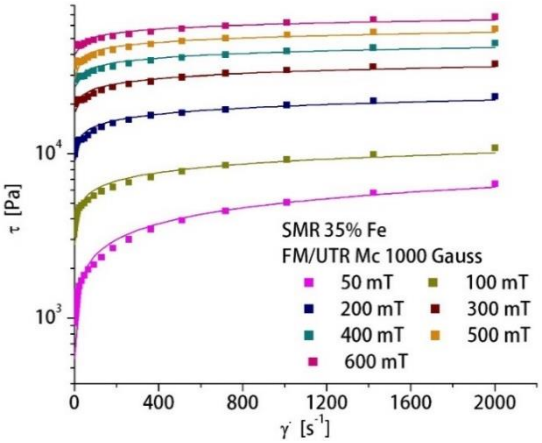

Figure 4. Flow curves for SMR 35% Fe + UTR Ms 1000 G – fitted with Power Law model.

B [mT]	*c*	*p*	$\mathbf{R^2}$
50	555.17	0.3188	0.9999
100	2772.55	0.17	0.9991
200	8336.608	0.123	0.997
300	15640.86	0.1009	0.999
400	21912.66	0.092	0.9978
500	33419.97	0.075	0.9994
600	39457.93	0.07	0.998

Table 1. Fitting parameters for designing the magneto-rheological torque contribution.

Due to the availability of the MRFs and the magneto-rheological behaviors 2 (MRF 132 DG and SMR 35% Fe + UTR Ms 1000 G) out of 4 initially selected fluids were further used. Using the fitting parameters (such as that from Table 1), the magneto-rheological torque contribution was computed and presented into the manuscript. Figure 5 shows the magneto-rheological braking torque [Nm] against the magnetic flux density B [mT] for the two selected MRF`s.

In this way the magneto-rheological torque contribution of the designed device was obtained. Differences of less than 5% resulted between the values obtained with equation (1) with respect to equation (2). The standard deviation is represented on the obtained data using vertical bars. The standard deviation was obtained from the random uncertainties of measurements of magneto-rheological experiment.

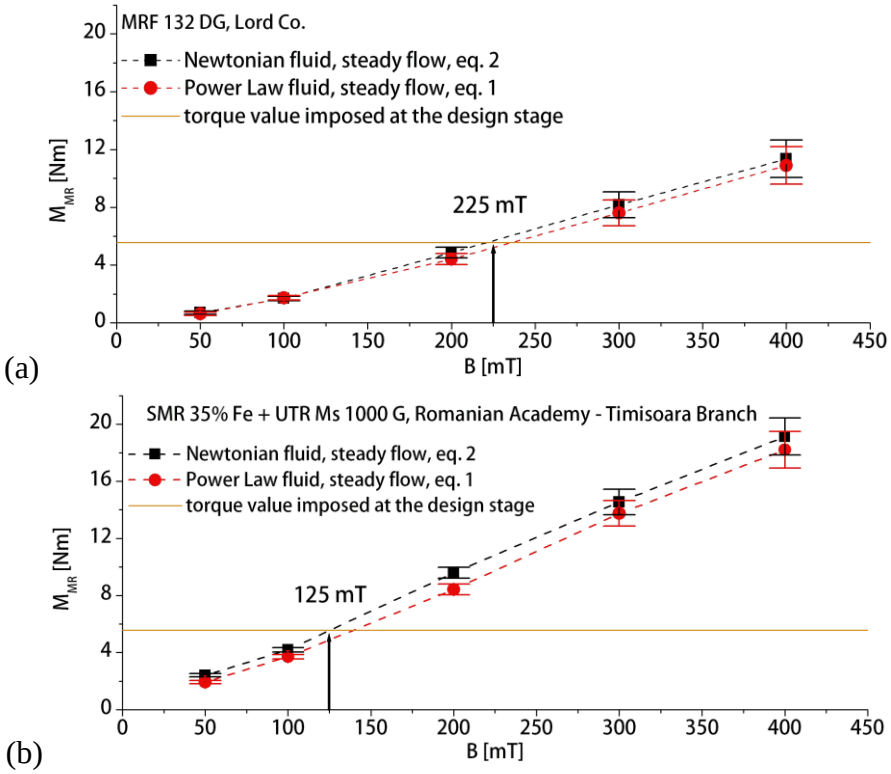

Figure 5. The calculated magneto-rheological torque contribution for MRF 132 DG (a) and SMR 35% Fe + UTR Ms 1000 G (b).

The underlined results at the end of Chapter 2 show that the SMR 35% Fe + UTR Ms 1000 G produced by the Magnetic Fluids Laboratory of the Romanian Academy – Timisoara Branch has better performances in terms of magneto-rheological behavior and reaching the torque value imposed at the design stage than MRF 132 DG produced by Lord Corporation. Using the SMR 35% Fe + UTR Ms 1000 G, the magnetic flux density to reach 5.57 Nm is 40% lower than with MRF 132 DG.

Next, in **chapter 3** the design methodology is validated against experimental data obtained with a 1:1 scale device as the one designed to control the rotor`s speed of the swirling flow generator. This part of the manuscript presents experimental investigations conducted to validate the design methodology and explore the operation of the designed device in both air and underwater working environments.

This analysis was performed on the test rig for testing magneto-rheological devices developed by Dr. Bosioc available at Faculty of Mechanics of Politehnica University Timisoara. The testing rig is presented in Figure 6. The testing rig allows to control the speed of an electrical motor and record the braking torque using a torque sensor. The speed range of the electric motor has been set in agreement with the rotor`s speed of the swirling flow generator. The range of the analyzed

regimes is from 100 to 1100 rpm with a 100 rpm increment. Due to a plexiglass section mounted over the magnetorheological speed control device, underwater testing has been possible.

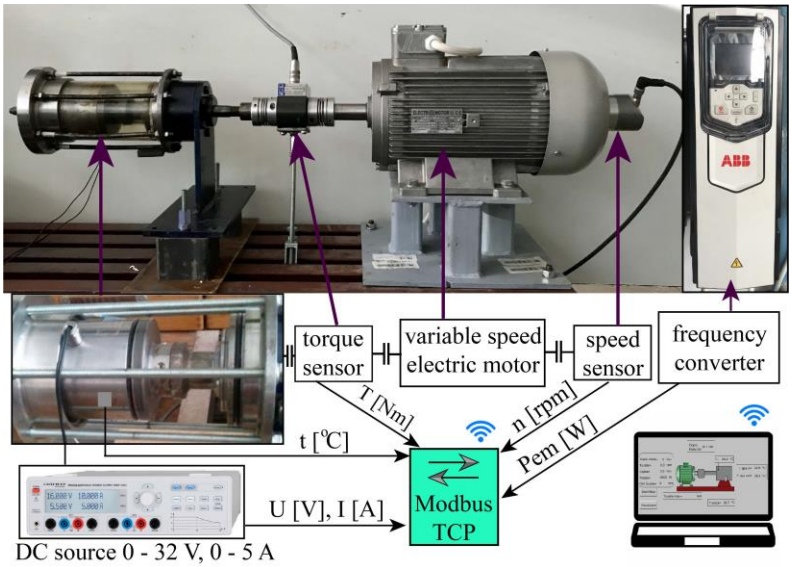

Figure 6. Test rig to assess MRB's performances available at Politehnica University Timisoara.

Next, tests were performed using the MRFs selected in the previous chapter and the results are presented and discussed. The variation of the magneto-rheological braking torque (M mr) is then presented against the magnetic flux density B. Examples of these results are presented in Figure 7. The data is presented comparatively for working with the two selected MRFs in air and water working environment. To plot the graph considering the same quantity on the abscissa, the correlation of the power applied to the coil and the magnetic flux density has been determined experimentally. Gauss FW Bell 5040 with Hall probe was used. The experimental results for all investigated points are represented with dots on the graph and the first order polynomial that presents the tendencies are represented with straight lines. The red line represents the torque value imposed at the design stage.

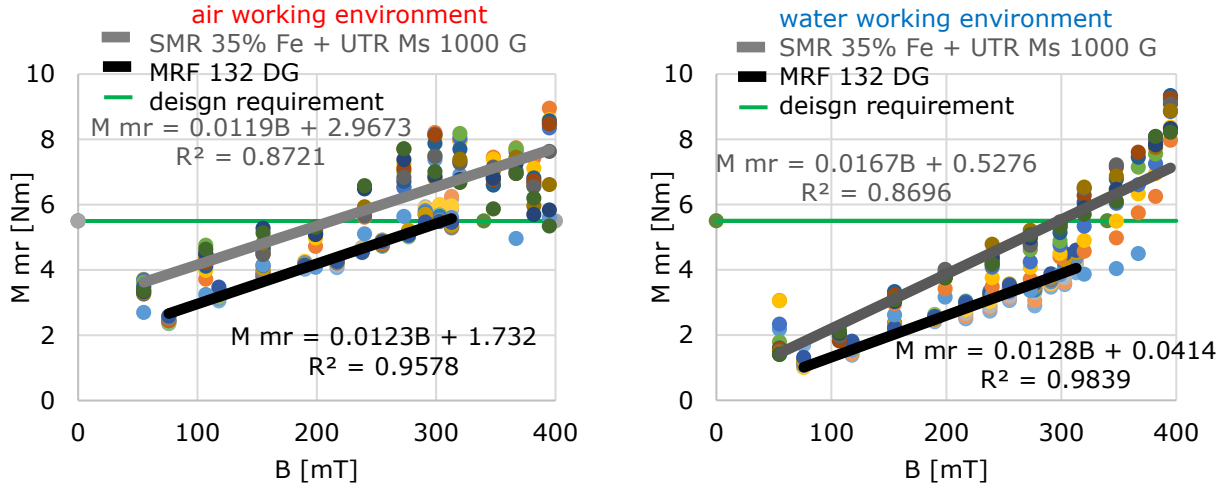

Figure 7. Magneto-rheological torque contribution variation against the magnetic flux density for the two selected MRFs while operated with the designed device in air (a) and water (b) working environment.

While operated underwater, SMR 35% Fe + UTR Ms 1000 G reaches the torque value imposed at the design stage at about 300 mT magnetic flux density in probe, see Figure 7b. During the experimental measurements campaign, MRF 132 DG showed a strong wash away phenomenon

of the iron particles and does not reach the 5.57 Nm torque contribution. For this reason, it is not recommended to use MRF 132 DG in applications that operate underwater.

While operating in air working environment, both MRFs reach 5.57 Nm, see Figure 7a. These experimental points are then used to validate the design methodology, Figure 8. At this stage, in the design methodology a correction of active height of the device`s gap (0.7h) identified from experimental investigations performed with the Hall probe is implemented. The correction leads to a better approximation of the magneto-rheological torque contribution with the developed relation, equation (1). The initially designed magneto-rheological torque is represented with dashed lines and squares in black / dash lines and circles in red, the corrected values are represented with solid lines and half empty in black / solid line and half empty rounds while the experimental data are plotted in black squares.

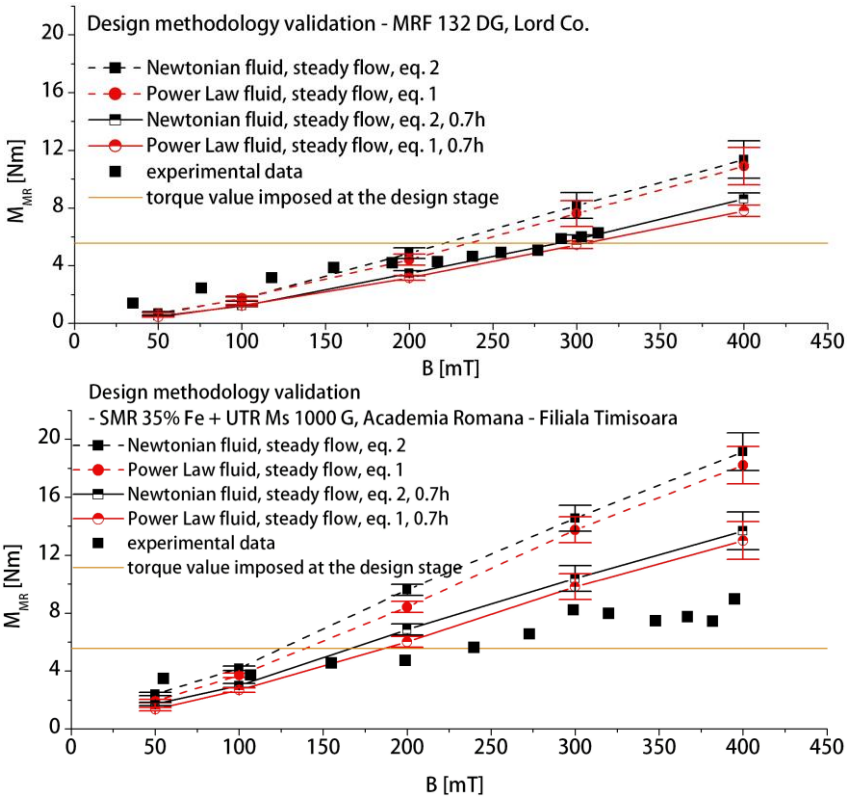

Figure 8. Checking of the calculated magneto-rheological torque contribution against experimental data for MRF 132 DG (a) and SMR 35% Fe + UTR Ms 1000 G (b).

Next, the analysis of the performances of the magneto-rheological control device is presented. The braking torque caused by the friction of the mechanical parts (M mec), the electromagnetic braking torque (M em) and the magneto-rheological braking torque (M mr) contribution in the total braking torque are studied. In general, all these investigations show that the biggest contribution belongs to the magneto-rheological braking torque and vary between 58% to 85% out of the total braking torque for both air and water working environments. In particular, when operating the device underwater with SMR 35% Fe + UTR Ms 1000 G, the magneto-rheological braking torque contributes 70-85% of the total braking torque. For this reason, the nano-micro composite called **SMR 35% Fe + UTR Ms 1000 G has been selected to control the rotor`s speed of the swirling flow generator.**

Using the designed magneto-rheological device and selected MRF, experimental analysis of the hydrodynamic flow field at several operating points of the swirling flow generator has been done in **chapter 4.** The experimental test rig for decelerated swirling flow together with the designed flow

control device embedded in the rotor hub has been used [27]. Seven operating points of the swirling flow generator were obtained breaking the rotor speed from 1020 rpm to 800 rpm. These investigations were performed in a straight configuration by a 2 m straight pipe mounted at the outlet of the test section.

The morphology of the vortex rope generated by the swirling flow generator is similar with the ones at part load conditions presented in Figure 1. While the rotor of the swirling flow generator spins freely at around 1020 rpm, the associated phenomena from the divergent part of the test section are similar with the ones from Francis FLINDT hydraulic turbine operated at 70% out of BEP. By reducing the rotor`s speed to 800 rpm, the flow regimes are improved. The quantitative improvement was assessed using the Fast Fourier Transform on the unsteady pressure signals measured at the wall of the test section, downstream of the braked swirling flow generator`s rotor. The 3D waterfall diagrams of the decomposed power spectra of the pressure signals for MG1 measuring level (placed in the conical area of the test section) and AM measuring level (placed upstream to the swirling flow generator) are presented in Figure 9 for 7 operating points.

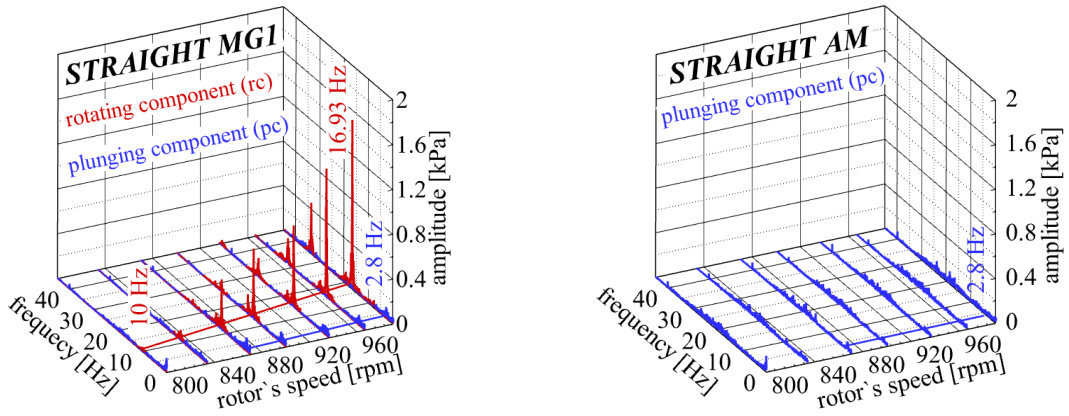

(a)

Figure 9. 3D waterfall diagrams of the decomposed power spectra of the pressure signals (plunging – blue and rotating - red) acquired on the test section levels for variable operating conditions: (a) MG1, (b) AM.

The decomposed power spectra analysis identifies two types of pressure pulsations: the rotating type component marked with red (caused by the precession motion of the instability) and the plunging type component marked with blue (caused by the self-excitation of the flow). The rotating type component acts locally in the draft tube cone [3] while the plunging one propagates as a shock wave in the entire hydraulic circuit [28]. Such a plunging component propagating in the hydraulic circuit may interact with other frequencies and lead to resonance [29]. From this reason, special attention was given to this component in chapter 6 to better understand its source. However, by controlling magneto-rheologically the rotor`s speed of the swirling flow generator at 800 rpm, both frequencies and associated amplitudes of the pressure pulsation are diminished by more than 90%. This is a consequence of the braking speed of the rotor being the only modified parameter during investigations.

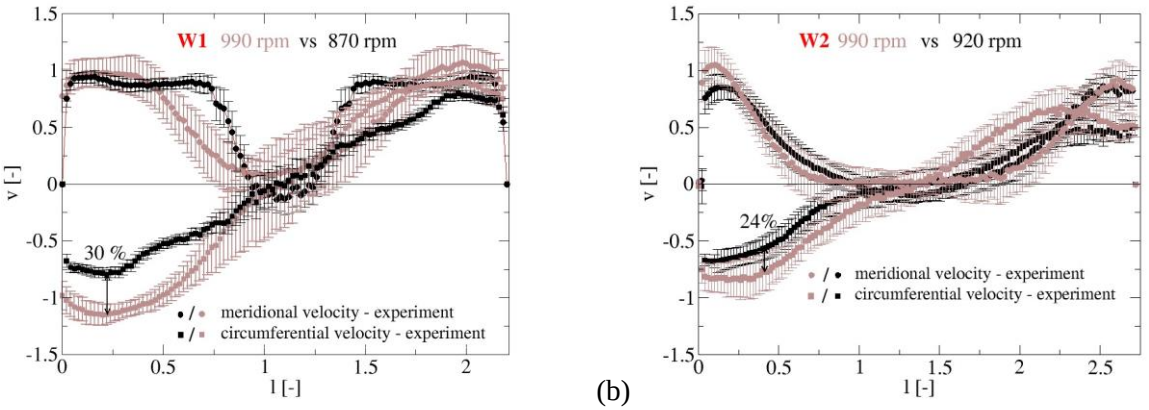

(a) (b)

Figure 10. Mean velocity profiles on the meridional and circumferential velocity components experimentally measured on W1 axis (a) at 990 rpm (grey) vs. 870 rpm (black) and on W2 axis (b) at 990 rpm (grey) vs 920 rpm (black).

Also, the mean velocity profiles of meridional and circumferential components are measured downstream of the braked rotor, see example in Figure 10. From the literature is well known that this flow topology is characterized by a central quasi stagnant region and strong circumferential velocity [18]. Hence, the influence of the rotor`s speed on the stagnant region and swirling flow has been assessed using 2D LDV measurements. In the manuscript are studied the mean velocity profiles of the above-mentioned components on the measuring axis in the convergent region (W0, see Figure 2) and in the divergent region (W1 and W2, see Figure 2). The results shows that while the rotor speed is braked:

- the quasi-stagnant region identified in the mean velocity profile of meridional component decreases with about 30% from 0.3 to 0.1 from the total axis length when the rotor speed is braked from 990 rpm to 870 rpm.
- the strong peripherical swirling flow identified in the mean velocity profile of circumferential component decrease by up to 30% on W1 with the rotor`s speed braked from 990 rpm to 870 rpm and decrease by up to 20% on W2 with the rotor`s speed braked from 990 rpm to 920 rpm.

Using numerical investigations, in **chapter 5**, the same operating points investigated experimentally were studied. The four domains of the swirl generator were considered separately and coupled together using a Mixing Plane method. Thus, between each two successive domains a mixing plane (MP) was defined to transfer and couple the flow, Figure 11. At the inlet side, I imposed a discharge of 30 l/s as in experimental investigation. The discharge is given by the 1.7045 m/s axial velocity. For turbulence specification method we used intensity and hydraulic diameter where the turbulent intensity is 3.376% and the hydraulic diameter is 0.15 m. The turbulent intensity was calculated using the following formula $I = 0.16(Re_{DH})^{-1/8}$ [30].

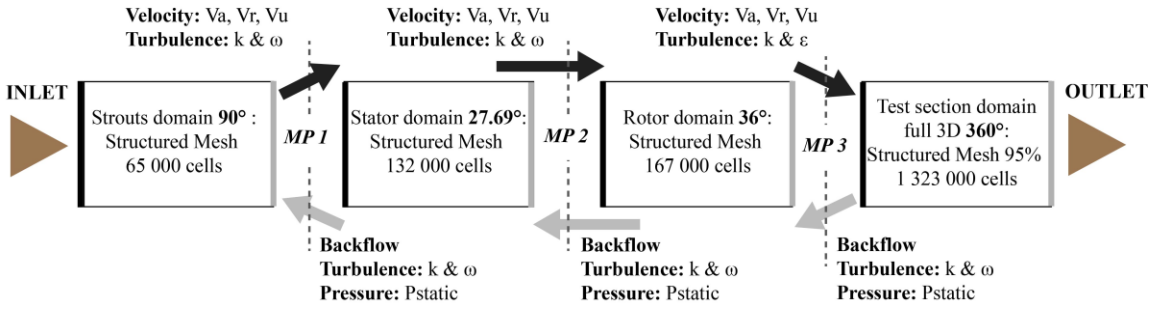

Figure 11. The mixing planes (MP1, MP2 and MP3) created between swirl apparatus domains.

Leaned strouts, guide vane and rotor domain were simplified in agreement with geometrical symmetry and periodical flow behavior. Therefore, from the leaned strouts domain, 90°=2π/4 was built, 27.69°=2π/13 from the guide vane and 36°=2π/10 from the rotor. An absolute steady state numerical simulation was performed on the leaned strouts and guide vane domain and relative steady state numerical simulation for the rotor. Due to unsteady phenomena expected in the 360° convergent-divergent test section an unsteady state numerical simulation was performed. For the flow simulation of leaned strouts, guide vane and rotor domain RANS equations were solved together with k-ω standard turbulence model. For convergent-divergent test section the RSM model has been chosen because the features of unsteady field are better captured [31].

The aim of this numerical experiment is to validate the work methodology and to use the results of the numerical investigation in Chapter 6 to study the vortex rope morphology. Flow couple and transfer between the domains of the swirl generator is checked for the numerical investigated operating regimes with the rotor speed of 1020, 990, 960, 920, 870 and 820 rpm, respectively. On each interface the global quantities of the volumetric flow rate and the flux of moment of momentum are checked then the relative error is calculated. The relative errors of volumetric flow rate and flux of moment of momentum versus the rotor speed are plotted in Figure 5a, b.

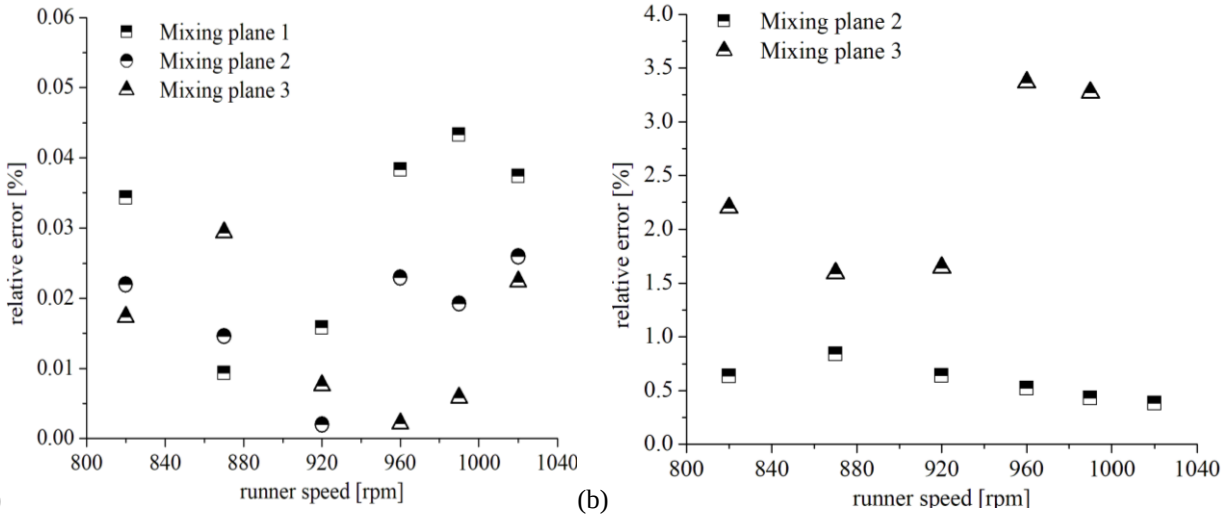

Figure 11. The quantities (volumetric flow rate and flux of moment of momentum) checked on the mixing planes to conserve the operation point.

The parameters of the operating points are conserved on all three mixing planes. The volumetric flow rate is conserved to a limit of a relative error of 0.043% while the flux of moment of momentum with about 3.5%. Hence, the operating point was conserved during numerical investigation in agreement with the checking procedure above-mentioned.

Next, the mean velocity flow field and the unsteady pressure pulsation numerically obtained were validated against the experimental data. The mean velocity profiles of meridional and circumferential component were compared with experimental data as follows:

- on the measuring axis corresponding to W0 window at rotor`s speed of 990, 960, 920, 870 and 800 rpm.
- on the measuring axis corresponding to W1 window at rotor`s speed of 990, 960, 920 and 870 rpm.
- on the measuring axis corresponding to W2 window at rotor`s speed of 990, 960 and 920 rpm.

A validation example is provided in Figure 13a for the results on the measuring axis corresponding to the W1 measuring window where the mean velocity profile of meridional and circumferential components obtained from the CFD are plotted against experimental data at 870 rpm.

The profiles obtained from the numerical investigation reproduce the experimental data in the limits of the fluctuation given by the root mean square of the experimentally measured velocity.

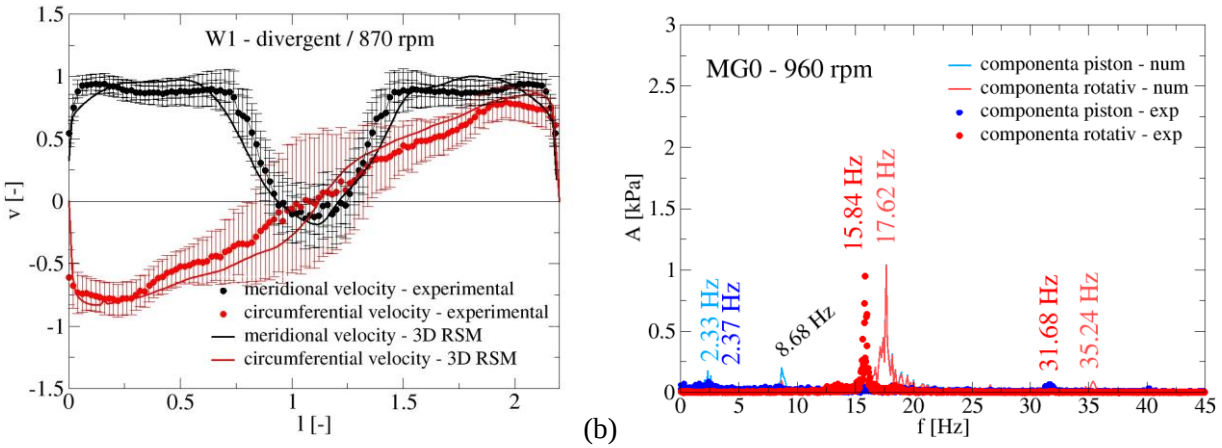

(a) (b)

Figure 13. Validation example of the mean velocity field (a) and the unsteady pressure field (b)

The unsteady pressure field from the CFD was also validated with experimental data on MG0, MG1, MG2 and MG3 measuring levels comparing the decomposed power spectra of the pressure signals. The rotating type frequency component was identified from numerical results at 18.42Hz, 17.62 Hz, and 12.64 Hz for rotor`s speed of 990, 960 and 870 rpm, respectively. A validation example of the unsteady pressure field is presented in Figure 13b. As it can be observed, the 3D numerical simulation with RSM turbulence model describes reasonably both the mean velocity field and the unsteady pressure one. This technique is reasonable from a computing resource and obtained results point of view. Hence, these results will be further used in chapter 6 to describe the vortex rope morphology in time for different operating regimes to study the low frequency plunging component source.

Chapter 6 extends the hydrodynamic flow analysis using the 3D numerical simulations results validated with experimental data. The vortex rope and associated vortex core morphology has been studied for operating points at 800, 870 and 920 rpm. The vortex rope filament was extracted for about 100 time steps at each operating point. Using the 3D logarithmic spiral model proposed by Stuparu and Resiga [32], the vortex core filament was reconstructed. The 3D logarithmic spiral model is described by the following geometrical parameters:

- b0/b1 – location of the cone apex corresponding s = 0;
- b1/a1 – cone half-angle γ; tan γ = b1/a1;
- a0 – arbitrary origin of the axial coordinate;
- c0 – phase, i.e., precession angle;
- c1 – helix pitch.

The parameters related to the evolution of the vortex core filament are presented for a random time step in Figure 14. The vortex rope is represented with iso-pressure colored in red while the vortex core filament is colored in blue.

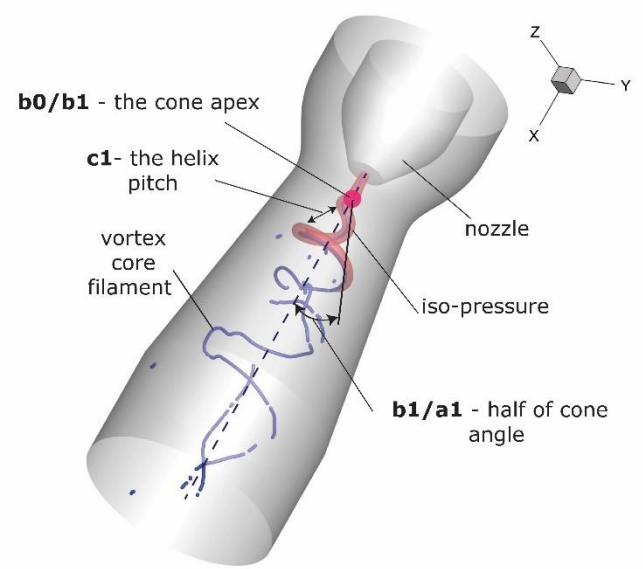

Figure 14. The vortex rope and associated vortex rope filament downstream to the rotor of the swirling flow generator

FX_VORTEXCORE routine implemented in commercial software TecPlot [33, 34] has been used for extracting the vortex core filaments from the numerical results. In this way, the x(s), y(s), z(s) and r(s) coordinates were obtained. The spurious segments were then removed (segments that are not related to the vortex core filament) and the points for increasing axial coordinate have been selected. Hence, clearly just a certain interval out of the total extracted vortex rope filament has been fitted.

A typical fit for the 3D vortex rope filament is presented in Figure 15. On the left side it can be observed that the x(s), y(s), z(s) and r(s) geometrical parameters are closely described by the model. On the right side, the 3D logarithmic spiral fit is plotted with red on the extracted vortex rope filament colored in blue. A good reproduction could be observed.

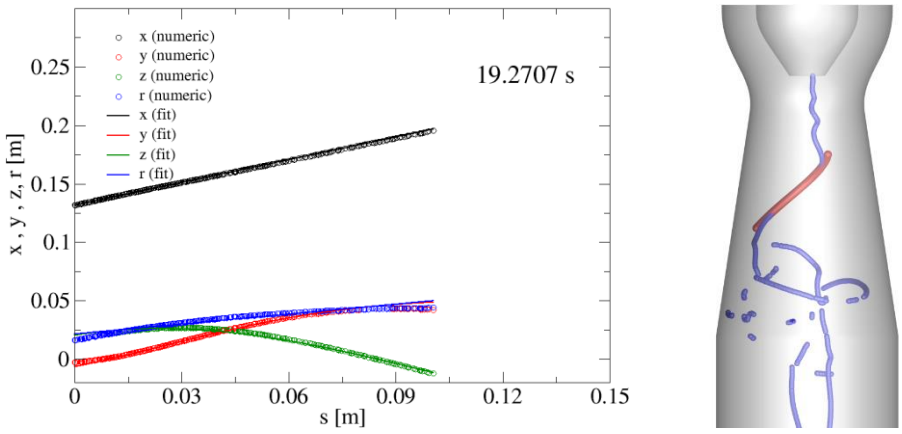

Figure 15. Least-squares fit of the numerical results validated with experimental data for the x(s), y(s), z(s) and r(s) coordinates corresponding 3D reconstruction of the vortex core filament for a time step at 870 rpm operating point.

The parameters that describe the 3D reconstructed logarithmic spiral were next used to assess the unsteady vortex rope morphology for more than 100 time steps for each operating point. The aim of these investigations was to quantify the maximum amplitude of each function of operating point. This amplitude is given by the maximum amplitude of the following periodic function:

$$f(t) = F_0 + F_1 \sin\left(\frac{2\pi}{T}t\right) + F2\cos\left(\frac{2\pi}{T}t\right) \quad (3)$$

where F_0, F_1, F_2 are obtained by fitting the numerical data, and $T = \frac{1}{f}$ is the time associated with the plunging and rotating type frequency for the investigated operating points.

The F amplitude is given by the following relation $F = \sqrt{F_1^2 + F_2^2}$. A typical representation for the studied parameters for 920 rpm is presented in Figure 16.

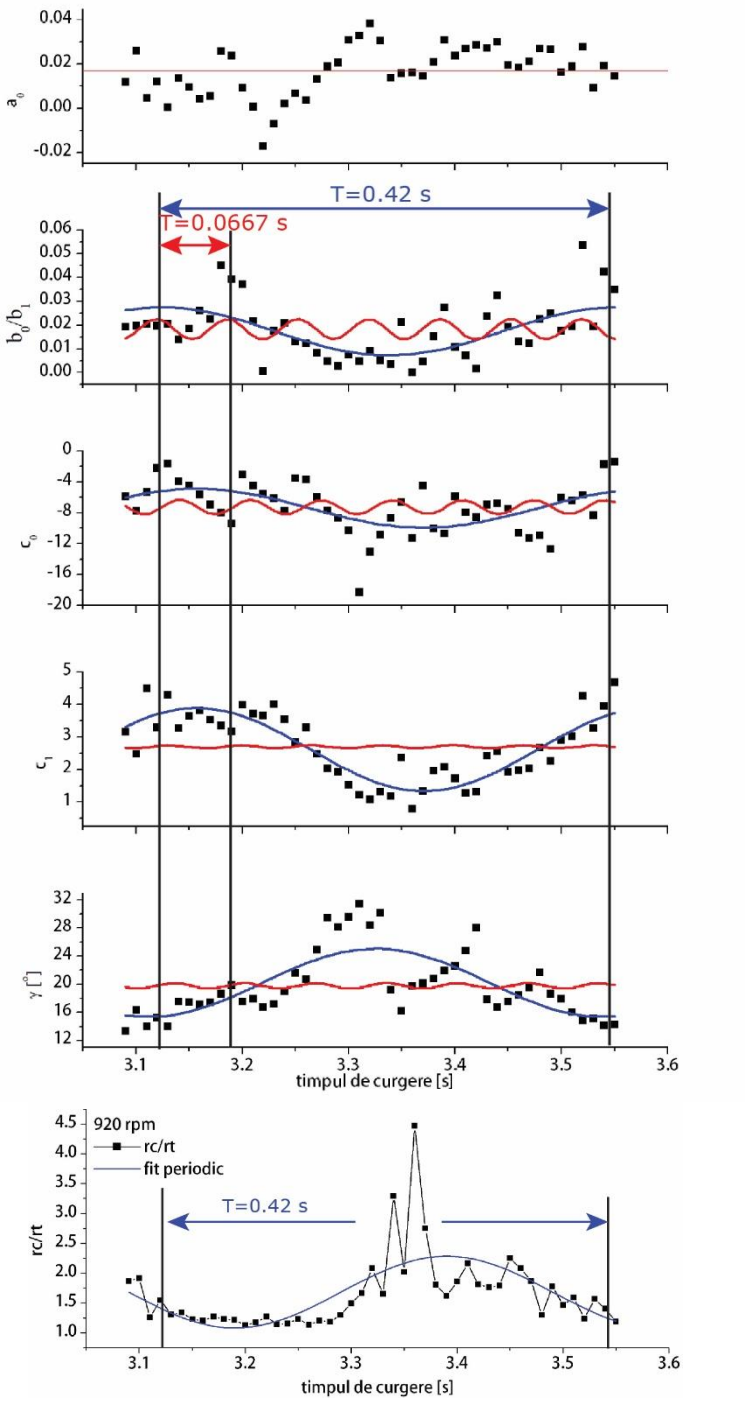

Figure 16. The parameters that describe the 3D reconstruction of the vortex core filament in time for 920 rpm operating point: a0 – arbitrary origin of the axial coordinate, b0/b1 – location of the cone apex corresponding s = 0, c0 – phase, i.e., precession angle, c1 – helix pitch, b1/a1 – cone half-angle γ; tan γ = b1/a1 and rc/rt – the ratio of the curvature and torsion radii

Colored in blue is presented the fitting obtained with equation (3) on the time period associated with the low frequency plunging component (e.g. γ for T ≈ 0.42s) and colored in red for the time period associated with the rotating frequency component. The evolutions evidenced by the equation (3), with the period associated with the low frequency plunging component shows that b0/b1, c0 and c1 parameters has the same phase tendency for all analyzed regimes. The γ parameters vary in opposite phase for all investigated points, except 870 rpm.

A0 parameter – is the arbitrary origin of the axial coordinate. This parameter fluctuates around a mean value for all investigated operating points. The highest value has been obtained at 870 rpm operating point.

B0/b1 parameter – gives the position of the cone apex on which the logarithmic spiral wraps. The small value of this parameter represents that the cone apex is situated close to a relative spot (e.g., nozzle`s tip), while the big values represent the opposite. The tendencies evidenced by equation (3) on the b0/b1 parameter show that the cone apex has a complete evolution, going up and down, in a period associated with the plunging type pressure pulsation.

C0 parameter – is the parameter that describes the phase changing (precession angle of the vortex core filament). The same tendency as for b0/b1 was obtained. In the first half of the period associated with the plunging component, the precession angle decreases while in the second half increases. The same effect was observed for all investigated operating points except for 800 rpm.

C1 parameter – gives the helix pitch. In other words, this parameter signals a compressed or an elongated 3D logarithmic spiral. The small values of this parameter show an elongated spiral while the big values show the opposite. In the first half of the period, the helix pitch increases while in the second part decreases. This parameter also has a complete evolution in a period associated with the low frequency plunging type pressure pulsation.

γ parameter – is the cone half-angle on which the vortex rope filaments wrap. This angle is obtained with the following equation: $\tan(\gamma)=b1/a1$. This parameter has an inverse variation than the other discussed above. The γ angle increases, while the position of the cone apex moves from upstream to downstream. This movement is complete after a period associated with the low frequency plunging type pressure pulsation.

Rc/rt ratio – identify the ratio between the curvature and torsion radii of the vortex core filament. This movement is complete after a period associated with the low frequency plunging type pressure pulsation in agreement with fitting realized.

To summarize, at 920 rpm operating point, in the first half of the period associated with the low frequency plunging component the morphology of the vortex rope:

- the cone apex gets closer to the nozzle`s tip (movement described by the b0/b1 parameter);
- the precession angle decrease (movement described by the c0 parameter);
- the helix pitch decrease (movement described by the c1 parameter);
- the half-angle cone increases (movement described by the γ parameter).

In the second half of the period associated with the low frequency plunging component, the cone apex moves away from the nozzle`s tip, the precession angle increases, the helix pitch increases and the half-cone angle increases. This mechanism has a complete evolution on the period associated with the low frequency plunging type pressure pulsation. This description is also available for the 800 rpm operating point. For 870 rpm operating point, the tendency evidenced by equation (3) differs just by the half-angle cone evolution which decreases in the first half and increases in the second half of the period associated with the low frequency plunging type pressure pulsation.

Next, using the mean values of each parameter and amplitude, the results evolutions with the operating point are studied. A typical result is presented in Figure 17 for the cone apex (b0/b1) and half-angle cone evolution with rotor`s speed from 920 to 800 rpm. With black squares are represented the mean values of the parameters while with vertical bars the amplitude.

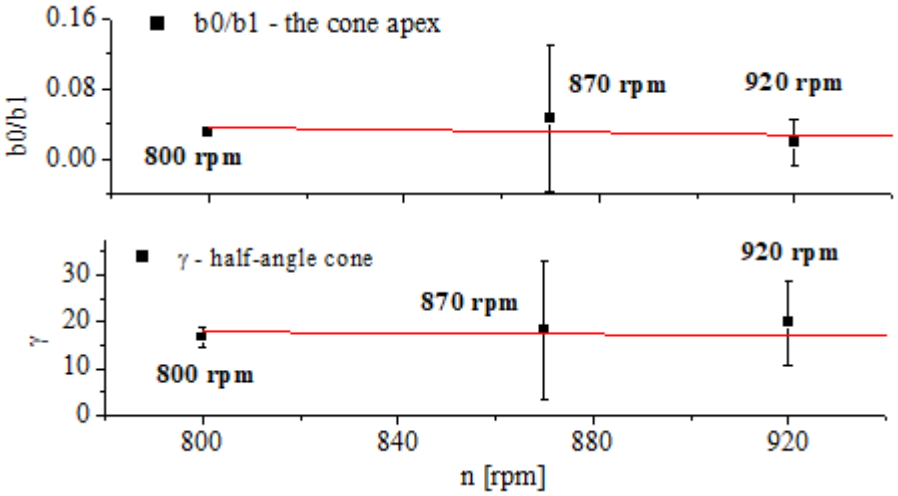

Figure 18. The cone apex and half-angle cone evolution with the operating point from 920 to 800 rpm

To identify the mechanisms that leads to the plunging type pressure pulsations in swirling flows in straight configurations, the mean values of each above mentioned parameter and associated amplitudes has been analyzed. The biggest amplitudes were obtained at 870 rpm operating point. In the manuscript these maximum values of the amplitudes are identified for the cone apex (given by the b0/b1 ratio), half-angle cone and the rc/rt ratio also at 870 rpm. The cone apex is a parameter correlated with the stagnant region. Hence, it can be said that the stagnant region evolution given by the amplitude of b0/b1 parameter, is maximum for the 870 rpm operating point followed by the 920 and 800 rpm operating point, respectively. Due to the reduced flux of moment of momentum, at 800 rpm operating point, the flow instabilities are diminished. The half-angle cone evolution has a maximum amplitude also for 870 rpm operating point. The amplitude varies from 60° to 10° and 32° to 18° at 870 and 920 rpm operating points, respectively. In agreement with experimental data presented in Chapter 4, the highest amplitude of plunging type pressure pulsations was measured at this regime. However, the mean value of the half-angle cone remains almost unchanged modifying the operating regimes.

To conclude, the low frequency plunging type component in straight configurations is generated by complex mechanisms that work together. From the obtained results it was underlined that the cone apex location, the half-angle cone and stretching and compression successively of the vortex core filament completely evolve in a period associated with the low frequency plunging type pressure pulsation.

Chapter 7 of the PhD. thesis studies the influence of the simplified elbow shape on the unsteady pressure field in a simplified geometry of the draft tube. Several operating points are obtained in this chapter using the designed magneto-rheological control device. The 3 simplified elbow geometry are presented in Figure 19. The interaction of the part load associated phenomena with the elbow draft tube is known as ”*draft tube surge*” [9, 35-39].

The HE90 simplified heel elbow geometry is like the one installed in hydropower plants between 1910-1940 [40-43]. The 74 degree heel elbow geometry is similar to the one design back in the 60`s and installed in hydropower plants between 1960-1980 [44, 45]. These geometries have been selected for installing in hydropower plants due to simplicity of the constructive solution and cost [46]. The aim of these investigations is to bring new knowledge in understanding the unsteady flow phenomena developed in the cone, induced by two simplified draft tube elbows. Moreover, this study tries to give answers to the new selections of the geometries to improve flows behavior at part load conditions.

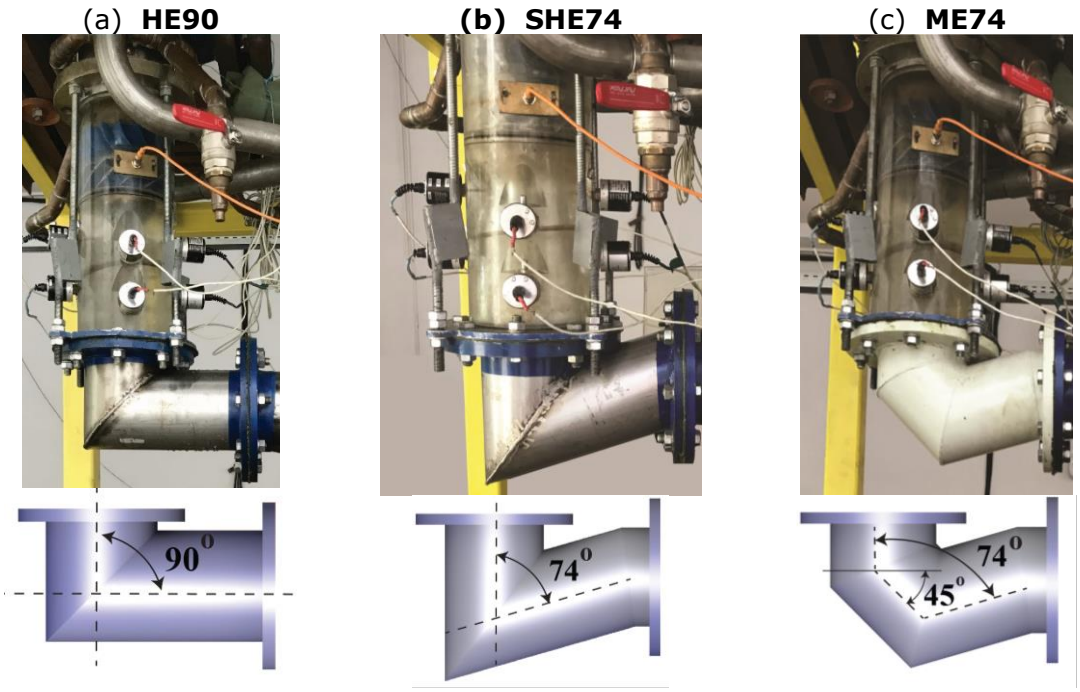

Figure 18. Photos and sketches of the simplified elbow draft tube geometries installed on test rig: (a) 90° Sharp Heel Elbow (HE90), (b) 74° Sharp Heel Elbow (SHE74), (c) 74° Modified Elbow (ME74)

The analyzing methodology was similar to the one used in straight configuration. In brief, the unsteady pressure signal has been decomposed (in synchronous and asynchronous component) and then the Fast Fourier Transform has been applied. In this way the decomposed power spectra of the unsteady pressure signals were obtained. This workflow leads to obtaining the main frequencies and associated amplitude of the pressure pulsations. The frequency associated with the rotating component was found at the same range as in straight configuration, suggesting that the processing motion of the flow instability is the same. Beside the low-frequency plunging component found in straight configuration, another plunging component caused by the swirling flow interactions with the elbow geometry has been found [47]. This frequency is ± 10% around 7.5Hz for the 3 analyzed geometries. It was shown that this component propagates upstream to the swirling flow generator with amplitudes with just 20% lower than the ones quantified into the cone.

The magneto-rheological control device for rotor`s speed of the swirling flow generator was successfully used to control the hydrodynamic regimes. The results studied comparatively for the 3 simplified draft tube heel elbows recommend a weak interaction of the swirling flow using a compact geometry with rounded edges, similar to ME74 geometry.

Chapter 8 presents the main conclusions, personal contributions and perspectives to continue the research. The results of the experimental and numerical investigations performed in the thesis were capitalized in 10 scientific papers. 2 scientific papers were published at *Energies (F.I – 3.252)* and *Proceedings of the Romanian Academy Series a-Mathematics Physics Technical Sciences Information Science (F.I. – 0.3)* journals. 6 scientific papers were published as Conference Proceeding in ISI (WOS) circuit and other 2 scientific papers in book chapter by *Ed. Springer* indexed in BDI (Scopus).

The main **personal contributions** were related to the development of a design methodology for magneto-rheological device to control the flow in the swirling flow generator and assessing the performance of it. Also, important contributions were obtained in term of analyzing the hydrodynamic flow field in the cone of hydraulic turbines in straight and with simplified heel elbows configurations. Hence, the following personal contributions can be listed:

- **elaboration of the magneto-rheological device design methodology** in double gap cylindrical configuration and validation with experimental data.
- **assessing the operation of the designed device** with MRF 132 DG and SMR 35% Fe + UTR Ms 1000 G both in air and water working environments.
- **experimental and numerical investigations** of the decelerated swirling flow **at several operating points** obtained **with the designed magnetorheological control device** in the swirling flow generator.
- **identifying the mechanism that work together and generates the plunging type pressure pulsations in straight configuration**.
- **experimental investigation** of the hydrodynamic pressure field in the cone of hydraulic turbine when **3 different simplified draft tube heel elbows** were **mounted downstream**.

The **perspectives** to continue the research program are the followings:

- Identification of new magneto-rheological fluids and their analysis in magneto-rheological devices operating in water;
- Identifying and correction of the deviation between the magnetic flux density considered in the design methodology and the resulted one, thermal field analysis and exploring different type of geometries to assess their impact on design methodology;
- The analysis of the vortex rope morphology in configurations with simplified heel elbow mounted downstream to the cone using 3D unsteady numerical simulations.

Bibliography

[1] Interantional Energy Agency. (2020, Noiembrie). Available: www.iea.org/fuels-and-technologies/renewables

[2] I. Kougias *et al.*, "Analysis of emerging technologies in the hydropower sector," *Renewable and Sustainable Energy Reviews*, vol. 113, p. 109257, 2019/10/01/ 2019.

[3] Y. Wu, S. Li, S. Liu, H. S. Dou, and Z. Qian, *Vibration of Hydraulic Machinery*. Springer Netherlands, 2014.

[4] D. Frunzăverde *et al.*, "Failure analysis of a Francis turbine runner," in *IOP Conference Series: Earth and Environmental Science*, 2010, vol. 12, p. 012115: IOP Publishing.

[5] T. Jacob, "Evaluation sur modèle réduit et prédiction de la stabilité de fonctionnement des turbines Francis " Phd Thesis 1993.

[6] S. Kumar, M. J. Cervantes, and B. K. Gandhi, "Rotating vortex rope formation and mitigation in draft tube of hydro turbines – A review from experimental perspective," *Renewable and Sustainable Energy Reviews*, vol. 136, p. 110354, 2021/02/01/ 2021.

[7] S. Pasche, F. Gallaire, and F. Avellan, "Origin of the synchronous pressure fluctuations in the draft tube of Francis turbines operating at part load conditions," (in English), *Journal of Fluids and Structures*, vol. 86, pp. 13-33, Apr 2019.

[8] X. Zhou, H.-g. Wu, and C.-z. Shi, "Numerical and experimental investigation of the effect of baffles on flow instabilities in a Francis turbine draft tube under partial load conditions," vol. 11, no. 1, p. 1687814018824468, 2019.

[9] D. Valentin, A. Presas, E. Egusquiza, C. Valero, M. Egusquiza Montagut, and M. Bossio, "Power Swing Generated in Francis Turbines by Part Load and Overload Instabilities," *Energies*, vol. 10, p. 2124, 12/13 2017.

[10] M. Nishi and S. Liu, "An Outlook on the Draft-Tube-Surge Study," *International Journal of Fluid Machinery and Systems*, vol. 6, 03/31 2013.

[11] M. Nishi, S. Matsunaga, T. Kubota, and Y. Senoo, *Surging Characteristics of Conical and Elbow-Type Draft Tubes*. 1984.

[12] M. Nishi, Matsunaga, S., Kubota, T., Senoo, Y., , "Flow regimes in an elbow-type draft tube," in *International Association of Hydraulic Research Symphosium* Amsterdam, Netherlands, 1982, vol. 2, no. 38, pp. 1-13.

[13] M. Nishi, X. Wang, K. Yoshida, T. Takahashi, and T. Tsukamoto, "An experimental study on fins, their role in control of the draft tube surging," in *Hydraulic machinery and cavitation*: Springer, 1996, pp. 905-914.

[14] K. Nakanishi and Ueda, "Air supply into draft tube of Francis turbine," *Fuji Electric Review*, vol. 10, no. 3, pp. 81-91, 1964.

[15] J. Kurokawa, H. Imamura, and Y.-D. Choi, "Effect of J-groove on the suppression of swirl flow in a conical diffuser," *Journal of Fluids Engineering*, vol. 132, no. 7, 2010.

[16] A. I. Bosioc, R. Szakal, C. Tanasa, and R. F. Susan-Resiga, "Experimental Investigation of a Free Runner Concept Downstream of Francis Turbines," in *IOP Conference Series: Earth and Environmental Science*, 2022, vol. 1079, no. 1, p. 012018: IOP Publishing.

[17] C. Tanasa, R. Susan-Resiga, S. Muntean, and A. I. Bosioc, "Flow-Feedback Method for Mitigating the Vortex Rope in Decelerated Swirling Flows," (in English), *Journal of Fluids Engineering-Transactions of the Asme*, vol. 135(6), no. 6, pp. -, Jun 2013.

[18] A. I. Bosioc, R. Susan-Resiga, S. Muntean, and C. Tanasa, "Unsteady Pressure Analysis of a Swirling Flow With Vortex Rope and Axial Water Injection in a Discharge Cone," (in English), *Journal of Fluids Engineering-Transactions of the Asme*, vol. 134, no. 8, Aug 2012.

[19] R. Susan-Resiga, T. C. Vu, S. Muntean, G. D. Ciocan, and B. Nennemann, "Jet control of the draft tube vortex rope in Francis turbines at partial discharge," in *23rd IAHR Symposium Conference*, 2006, pp. 67-80.

[20] R. Susan-Resiga, A. Stuparu, and S. Muntean, "Francis turbine with tandem runners: a proof of concept," in *IOP Conference Series: Earth and Environmental Science*, 2019, vol. 240, p. 022012.

[21] R. Resiga *et al.*, *SWIRLING FLOW APPARATUS AND TEST RIG FOR FLOW CONTROL IN HYDRAULIC TURBINES DISCHARGE CONE*. 2007.

[22] L. Vékás, "Ferrofluids and magnetorheological fluids," in *Advances in science and technology*, 2008, vol. 54, pp. 127-136: Trans Tech Publ.

[23] H. Nguyen and S. Choi, "Selection of magnetorheological brake types via optimal design considering maximum torque and constrained volume," *Smart Materials and Structures*, vol. 21, p. 015012, 12/20 2011.

[24] R. A. Szakal, S. Muntean, A. I. Bosioc, R. Susan-Resiga, and L. Vékás, "3D numerical investigations of the swirling flow in a straight diffuser for the variable speed values of the rotor obtained with a magneto-rheological brake," in *IOP Conference Series: Earth and Environmental Science*, 2021, vol. 774.

[25] J. F. Steffe, *Rheological methods in food process engineering*. East Lansing (Mich.): Freeman Press, 1992.

[26] H. M. Laun, C. Kormann, and N. Willenbacher, "Rheometry on magnetorheological (MR) fluids," *Rheologica Acta*, vol. 35, no. 5, pp. 417-432, 1996/09/01 1996.

[27] R. A. Szakal, A. I. Bosioc, S. Muntean, D. Susan-Resiga, and L. Vékás, "Experimental investigations of a magneto-rheological brake embedded in a swirl generator apparatus," in *Advanced Structured Materials* vol. 98, ed, 2019, pp. 265-279.
[28] T. L. Wahl, "Draft tube surging hydraulic model study, Master Thesis, Colorado State University, Fort Collins, CO, USA," 1990.
[29] X. Liu, Y. Luo, A. Presas, Z. Wang, and L. Zhou, "Cavitation Effects on the Structural Resonance of Hydraulic Turbines: Failure Analysis in a Real Francis Turbine Runner," vol. 11, no. 9, p. 2320, 2018.
[30] *Ansys Fluent Theory Guide, Release 15.0.* . 2013.
[31] S. Muntean, C. Tănasă, A. I. Bosioc, and D. C. Moş, "Investigation of the Plunging Pressure Pulsation in a Swirling Flow with Precessing Vortex Rope in a Straight Diffuser," in *IOP Conference Series: Earth and Environmental Science*, 2016, vol. 49, p. 082010: IOP Publishing.
[32] A. Stuparu and R. Susan-Resiga, "The Complex Dynamics of the Precessing Vortex Rope in a Straight Diffuser," (in English), *28th Iahr Symposium on Hydraulic Machinery and Systems (Iahr2016), Pts 1-12*, vol. 49, no. 2016, 2016 2016.
[33] D. N. Kenwright and R. Haimes, "Automatic vortex core detection," *IEEE Computer Graphics and Applications*, vol. 18, no. 4, pp. 70-74, 1998.
[34] R. Haimes and D. Kenwright, "On the velocity gradient tensor and fluid feature extraction," in *14th Computational Fluid Dynamics Conference*(Fluid Dynamics and Co-located Conferences: American Institute of Aeronautics and Astronautics, 1999.
[35] Rheingans, "Power swings in hydroelectric Power Plant," *Transactions of the American Society of Mechanical Engineers* vol. 6, pp. 171-184, 1940.
[36] J. J. Cassidy and H. T. Falvey, "Observations of unsteady flow arising after vortex breakdown," *Journal of Fluid Mechanics*, vol. 41, no. 4, pp. 727-736, 1970.
[37] H. T. Falvey, Cassidy, J.J., "Frequency and amplitude of pressure surges generated by swirling flows," presented at the International Association of Hydraulic Research Symposium on Hydraulic Machinery and System, Stockholm, Sweden, 1970.
[38] H. T. Falvey, "Draft tube surges," US Bureau of Reclamation Report REC-ERC-71-42REC-ERC-71-42, 1971.
[39] U. J. Palde, "Influence of draft tube shape on surging characteristics of reaction turbines," US Bureau of Reclamation Report REC-ERC-72-24 REC-ERC-72-24, 1972.
[40] T. F. Engstrom, Gustavsson, L.H., Karlsson R.I.,, "The second ERCOFTAC Workshop on Draft Tube Flow," ed. Alvkarleby, Sweden, 2001.
[41] M. J. Cervantes, Engstrom T.F., Gustavsson, L.H., "The third IAHR/ERCOFTAC Workshop on Draft Tube Flow ", ed. Porjus, Sweden, 2005.
[42] U. Andersson, "An experimental study of the flow in a sharp-heel Kaplan draft tube," 2009.
[43] N. Dahlbäck, "Redesign of Sharp Heel Draft Tube — Results from Tests in Model and Prototype," Dordrecht, 1996, pp. 985-993: Springer Netherlands.
[44] A. Baya, S. Muntean, V. C. Câmpian, A. Cuzmoş, M. Diaconescu, and G. Bălan, "Experimental investigations of the unsteady flow in a Francis turbine draft tube cone," in *IOP Conference Series: Earth and Environmental Science*, 2010, vol. 12, p. 012007: IOP Publishing.
[45] M. F. Gubin, *Draft Tubes of Hydro-electric Stations*. Amerind Publishing Company for the U.S. Bureau of Reclamation, 1973.
[46] S. Muntean, D. C. Moş, R. A. Szakal, A. I. Bosioc, and R. Susan-Resiga, "Influence of the elbow shape on the unsteady pressure field in decelerated swirling flows," in *IOP Conference Series: Earth and Environmental Science*, 2021, vol. 774.
[47] R. A. Szakal, A. Doman, and S. Muntean, "Influence of the reshaped elbow on the unsteady pressure field in a simplified geometry of the draft tube," *Energies*, Article vol. 14, no. 5, 2021, Art. no. 1393.